

EFFECT OF CONCENTRATION OF Mn DOPANT IONS ON THE STRUCTURAL AND OPTICAL PROPERTIES OF ZINC OXIDE CRYSTALS

F.I. EZEMA, U.O.A. NWANKWO

Department of Physics & Astronomy, University of Nigeria, Nsukka, Enugu State, Nigeria

Manganese (Mn) doped ZnO crystals have been successfully grown via the gel route. Identification of the chemical species of the crystals grown was done using Fourier Transform Infrared Spectroscopy (FTIR), structural analysis was done using X-Ray Diffraction technique while the optical properties were studied using UV-VIS technique. Results from the FTIR and XRD analysis show that high concentrations of manganese dopant ions results in the formation of synthetic MnO₂ (pyrolusite), degrading the quality of the ZnO crystals.

(Received December 9, 2010; accepted January 26, 2011)

Keywords: Mn doped ZnO, ZnO crystal, UV-Vis, FTIR, XRD, MnO₂

1. Introduction

Pure, undoped Zinc Oxide crystals have certain limitations in their application. In order to widen the potential areas where ZnO crystals can be applied, dopant ions have to be incorporated into them in order to obtain certain desired properties like wider or narrower band gap, higher optical absorbance, lower or higher melting point, ferromagnetism, etc.

Mn doped ZnO is regarded as promising material for spintronic applications as it shows room temperature ferromagnetism [1], and it has also been utilized as a material for the manufacture of solar cells, transparent electrodes, gas sensors, varistors, piezoelectric transducers, etc, due to its behaviour as a dilute magnetic semiconductor (DMS) [2]. DMS materials have many unique magneto-optical, magneto-electrical, and magneto-transport properties that are essential for future-generation spintronic device applications [3]. Mn-doped ZnO has been synthesized using atomic layer deposition (ALD) [2], sol-gel [4, 5], metal organic chemical vapour deposition (MOCVD) [6], ion implantation [7], pulsed laser deposition [8] and solid state sintering [9] methods.

In this study, Mn doped ZnO crystals were synthesized using the sol-gel technique. A gel is a colloidal system in which the dispersed substance forms a continuous, ramifying, space-enclosing framework. Sol-gel method is a wet chemical route for the synthesis of colloidal dispersions of oxides which can be altered to powders, fibres, thin films and monoliths [10] (see Fig. 1). Formation of crystals from the gel medium is achieved by creating a state of supersaturation in the gel medium either by evaporation or cooling.

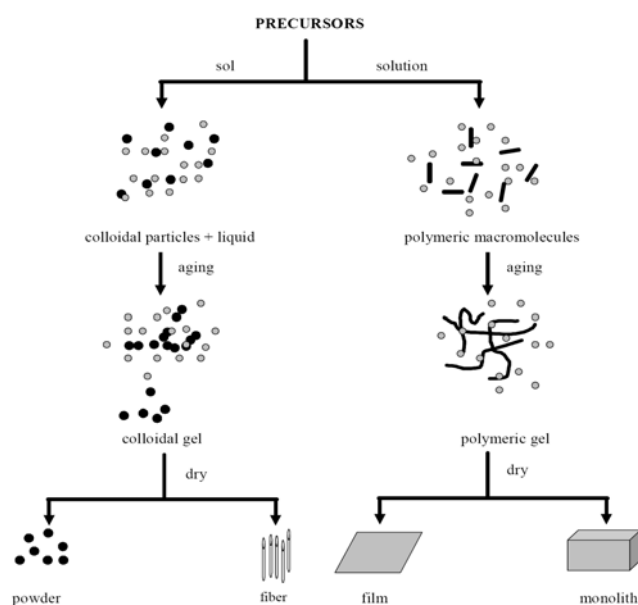


Fig.1. Schematic representation of the Sol-gel process [10]

2. Experimental details

For the synthesis of Mn-ZnO, absolute ethanol was used as solvent. Zinc acetate dihydrate $[\text{Zn}(\text{CH}_3\text{COO})_2 \cdot 2\text{H}_2\text{O}]$ was used as a source of both zinc and oxygen while manganese (II) acetate tetrahydrate $[\text{Mn}(\text{CH}_3\text{COO})_2 \cdot 4\text{H}_2\text{O}]$ was used as a source of the Mn^{2+} dopant ions. Zinc acetate dihydrate was used as source of both zinc and oxygen because it is known to be a 'mono-precursor' [11]. 10g of zinc acetate dihydrate was mixed with 25ml of absolute ethanol ($\text{C}_2\text{H}_5\text{OH}$) in a beaker. The resulting mixture was stirred using a magnetic stirrer for about 10 minutes. Then, 'X'g of manganese (II) acetate tetrahydrate $[\text{Mn}(\text{CH}_3\text{COO})_2 \cdot 4\text{H}_2\text{O}]$ was added to the solution. Addition of manganese (II) acetate tetrahydrate gave the solution an ash colouration. The solution was left to stir for another 20 minutes after which it was placed in an oven maintained at 104°C . Zinc acetate dihydrate and manganese (II) acetate tetrahydrate salts in the solution dissolved completely after about 70 minutes in the oven. Their dissolution released Zn^{2+} (from zinc acetate) and Mn^{2+} (from manganese acetate) ions into the solution. OH^- ions were also released from the organic components of the solution. These ions combined to yield the Mn-ZnO crystals.

Continuous heating resulted in the solution transiting to a state of supersaturation and the formation of a purplish gel. In this state of super-saturation, homogenous nucleation was enhanced and the crystal growth process was also sped up. Subjecting the gel to heat treatment (at 104°C) for up to 120 minutes ensured that the solvent and any moisture present were evaporated completely, leaving behind the manganese doped zinc oxide (Mn-ZnO) crystals. The crystals were then ground into finer particles using a mortar and pestle.

The 'X'g of manganese (II) acetate tetrahydrate mentioned above has values of 1g, 3g and 5g. The amount of manganese acetate was varied as shown in order to enable us investigate into the effect doping concentrations of manganese has on the structural property of zinc oxide.

3. Results and discussion

3.1 FTIR Analysis: FTIR is a technique used to obtain information about the chemical bonding in a material. It is used to identify the elemental constituents of a material sample. FTIR analysis was performed using SHIMADZU FTIR. For our study, the Double-Pass Transmission mode was used. Here, the infrared (IR) beam makes a double pass through the sample before reaching the detector. The double-pass mode was used because it offers the highest level of sensitivity [12].

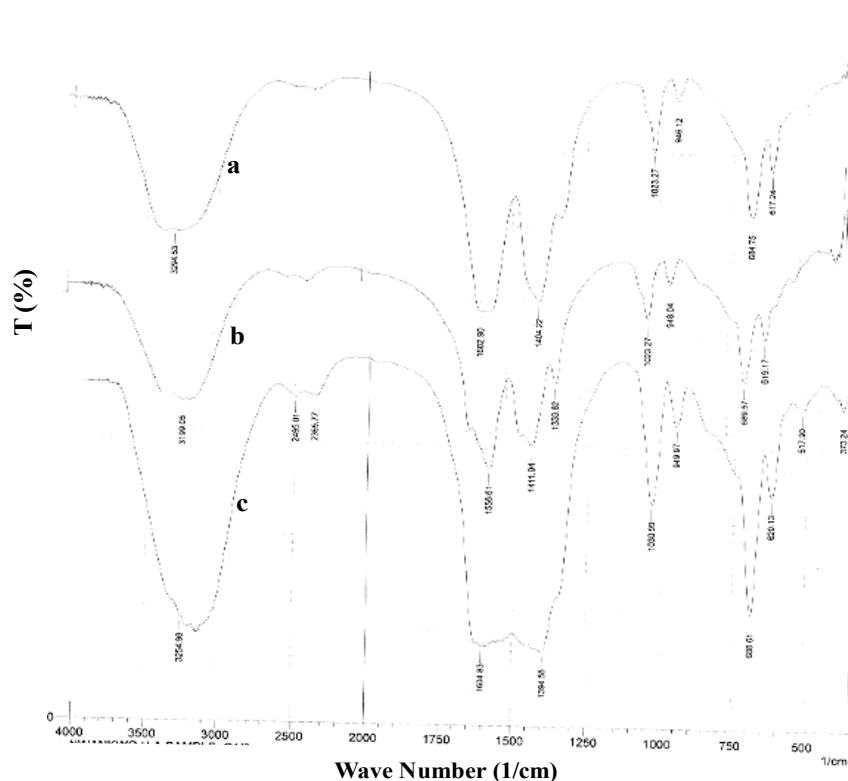


Fig. 2. FTIR Spectrum of Mn-ZnO crystals – (a) Grown with 5g Magnesium Acetate, (b) Grown with 3g Manganese Acetate, (c) Grown with 1g Manganese Acetate.

Fig. 2(a-c) above shows the FTIR spectra of Mn-ZnO crystals. In Fig. 2a, we observe various peaks corresponding to the main absorption bands. These absorption bands are due to ‘normal polymeric’ O-H stretching of the hydroxyl group at 3294.53cm^{-1} [13, 15]; O-H bending of the hydroxyl group at 1404.22cm^{-1} [13] and O-H out-of-plane bending of the hydroxyl group at 617.24cm^{-1} [13]; and an Mn-O stretching at 949.97cm^{-1} [15]. Fig. 2b shows various peaks corresponding to the main absorption bands. These absorption bands are due to ‘normal polymeric’ O-H stretching of the hydroxyl group at 3199.05cm^{-1} [13, 15]; O-H bending of the hydroxyl group at 1333.82cm^{-1} and 1411.94cm^{-1} [13]; O-H out-of-plane bending of the hydroxyl group at 619.17cm^{-1} [13]; and an Mn-O stretching at 948.04cm^{-1} [15]. Similarly, Fig. 2c shows various peaks corresponding to the main absorption bands which are due to ‘normal polymeric’ O-H stretching of the hydroxyl group at 3254.98cm^{-1} [13, 15]; O-H bending of the hydroxyl group at 1394.58cm^{-1} [13] and O-H out-of-plane bending of the hydroxyl group at 620.13cm^{-1} [13]; Zn-O stretching of ZnO at 373.24cm^{-1} [14]; and an Mn-O stretching at 949.97cm^{-1} [15].

From the FTIR spectra (Fig. 2(a-c)), we observe that increasing the amount of the dopant ion (Mn^{2+}) in the crystal resulted in the absence of IR peaks corresponding to Zn-O bonds in Fig. 2(a-b). This is probably due to a substitution of Zn^{2+} ions by Mn^{2+} ions in the crystal lattice structure.

3.2 Structural Analysis

XRD was used to uniquely identify the crystalline phases present in the crystals and to study the structural properties. The XRD analysis of crystal samples were carried out using MD-10 Diffractometer, which recorded diffractograms using $\text{CuK}\alpha$ radiation. Diffraction patterns of the samples were recorded in the 2θ range from 10° to 72° .

The XRD spectra in Fig. 3(a-f) below show that the samples are crystalline in nature. The crystallite size D , was determined using the Debye Scherrer formula [16, 17, 18, 19] as given below:

$$D = \frac{K\lambda}{\beta \cos \theta} \quad (1)$$

where $K = 0.9$, is the shape factor, $\lambda = 1.5408 \text{ \AA}$, θ is the diffraction peak angle (Bragg Angle) in degrees, and β denotes the full width at half maximum (FWHM) in radians, of the corresponding diffraction peak

For the spectrum of Mn-ZnO crystals grown with 5g of manganese acetate (see Fig. 3a), the diffraction peaks observed do not correspond to the hexagonal phase zinc oxide peaks. Observable from the spectrum is the peak at $2\theta^\circ = 27.78$ corresponding to the (110) plane of synthetic MnO₂ (pyrolusite), which is very stable with tetragonal rutile structure [20].

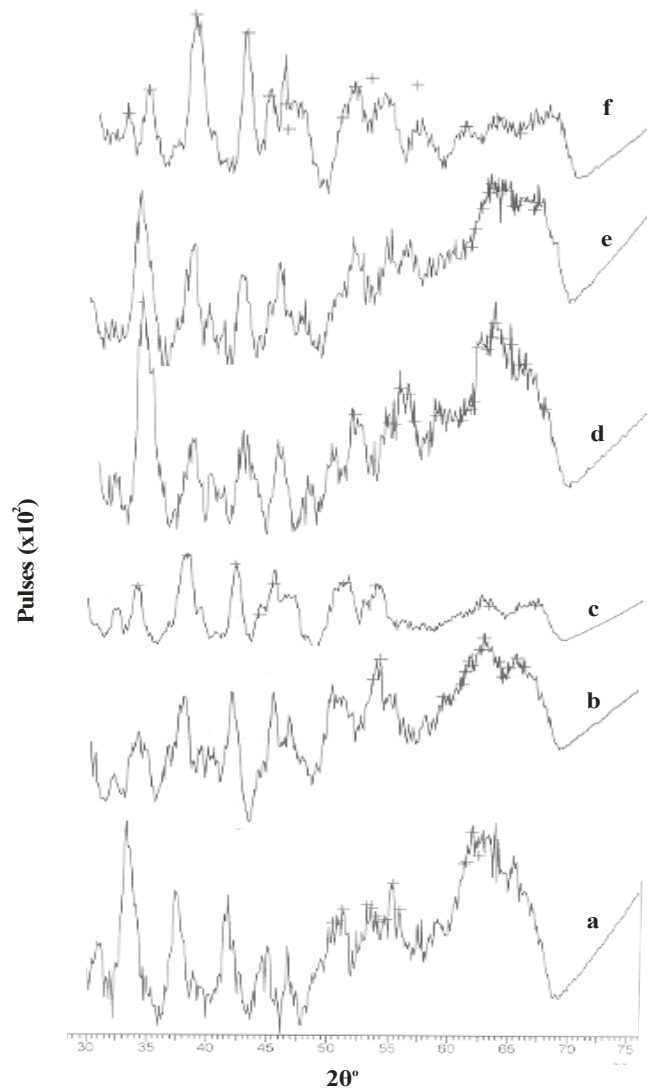


Fig. 3. XRD Spectrum for Mn-ZnO crystals – ‘a’ → for ‘X’g = 5g (as-grown), ‘b’ → for ‘X’g = 3g (as-grown), ‘c’ → for ‘X’g = 1g (as-grown), ‘d’ → for ‘X’g = 5g annealed for 30 minutes at 200 °C, ‘e’ → for ‘X’g = 3g annealed for 30 minutes at 200 °C, ‘f’ → for ‘X’g = 1g annealed for 30 minutes at 200 °C.

Fig. 3b shows the XRD spectrum of Mn-ZnO crystals grown with 3g of manganese acetate. Here we observe two peaks at $2\theta^\circ = 62.61$ for the (103) plane [21] and $2\theta^\circ = 65.94$ for the (200) plane [21], which corresponds to peaks characteristic of zinc oxide’s hexagonal wurtzite structure. The peak corresponding to the (110) plane of synthetic MnO₂ (pyrolusite) [20] was also observed at $2\theta^\circ = 28.43$.

Fig. 3c shows the XRD spectrum of Mn-ZnO crystals grown with 1g of manganese acetate. Various peaks at $2\theta^\circ = 33.75$ (002), $2\theta^\circ = 62.98$ (103) and $2\theta^\circ = 66.85$ (200) [21, 20, 5], corresponding to the hexagonal wurtzite structure of zinc oxide. Also observed in the spectrum is the peak at $2\theta^\circ = 28.37$, corresponding to the (110) plane of synthetic MnO₂ (pyrolusite) [20].

Shown in Fig. 3d is the XRD spectrum of Mn-ZnO crystals grown with 5g of manganese acetate and annealed for 30 minutes at 200°C. Diffraction peaks at $2\theta^\circ = 33.71$ for the (002) plane and $2\theta^\circ = 56.13$ for the (110) plane, corresponding to peaks characteristic of the hexagonal wurtzite structure of zinc oxide were observed [21, 20, 5]. Also observed in the spectrum is the peak at $2\theta^\circ = 27.58$, corresponding to the (110) plane of synthetic MnO₂ (pyrolusite) [20].

Fig. 3e is the XRD spectrum of Mn-ZnO crystals grown with 3g of manganese acetate and annealed for 30 minutes at 200°C. Diffraction peaks at $2\theta^\circ = 62.95$ for the (103) plane and $2\theta^\circ = 66.30$ for the (112) plane, corresponding to peaks characteristic of the hexagonal wurtzite structure of zinc oxide were observed [21, 20, 5]. In the spectrum, we also note the peak at $2\theta^\circ = 28.38$, corresponding to the (110) plane of synthetic MnO₂ (pyrolusite) [20].

Similarly, Mn-ZnO crystals grown with 1g of manganese acetate and annealed for 30 minutes at 200°C (Fig. 3f) shows diffraction peaks at $2\theta^\circ = 31.65$ for the (100) plane, $2\theta^\circ = 33.38$ for the (002) plane, $2\theta^\circ = 37.29$ for the (101) plane, and $2\theta^\circ = 62.26$ for the (103) plane, corresponding to peaks characteristic of the hexagonal wurtzite structure of zinc oxide were observed [21, 20, 5]. In the spectrum, we also note the peak at $2\theta^\circ = 28.05$, corresponding to the (110) plane of synthetic MnO₂ (pyrolusite) [20].

From the results of the XRD analysis of Mn-ZnO crystals, we observe that for Mn-ZnO crystals with higher concentrations of manganese dopant (i.e. crystals grown with mass of manganese acetate greater than 1g), their structure deviate from the hexagonal wurtzite structure of zinc oxide. This is evident due to the conspicuous presence of the peak corresponding to the (110) plane of synthetic MnO₂ (pyrolusite) and the absence of characteristic ZnO peaks (for the '002' plane in particular); and is in agreement with the observations from the FTIR spectra which show Zn-O bonds only for crystals grown with 1g manganese acetate.

3.3 Optical Studies

Optical absorption studies of the crystalline particle colloids were carried out using a JENWAY 6405 UV-VIS spectrophotometer operating at a wavelength range of 200nm to 1200nm at intervals of 5nm. In the optical absorption study, deionised water was used as reference solution [22]. First, the crystal samples were dissolved in deionised water forming a colloidal solution which is then subjected to UV-VIS analysis.

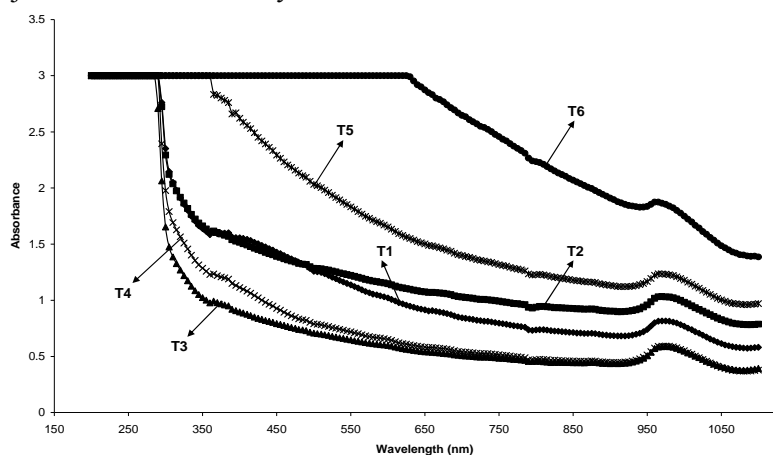


Fig. 4. Optical absorption spectra for as- grown and annealed Mn-ZnO.

From the optical absorption spectra shown in Fig. 4, we observe that increasing the doping concentration results in an increase in the absorbance of the crystal across all wavelength ranges of the visible region of the spectrum. This is seen when one compares the spectra for the as-grown samples - T3, T2, T1 (i.e. 1g, 3g, and 5g manganese acetate respectively); whereas the absorbance for the annealed samples - T6, T5, T4 (i.e. 1g, 3g, and 5g manganese acetate respectively) decreases with increasing dopant concentration.

Figures 5 and 6 below show the band gap and Urbach's energy respectively, for each Mn-ZnO crystal sample. Urbach's energy corresponds to the width of the tail of localised states within the optical band gap. It can be deduced from the absorption coefficient (α) and depends on structural defects [23]. It is determined by plotting $\ln(\alpha)$ against photon energy [24], and extrapolating to the photon energy axis. Variation of band gap and Urbach's energy with doping concentration as well as with annealing temperature is shown in Tables 1 and 2 respectively.

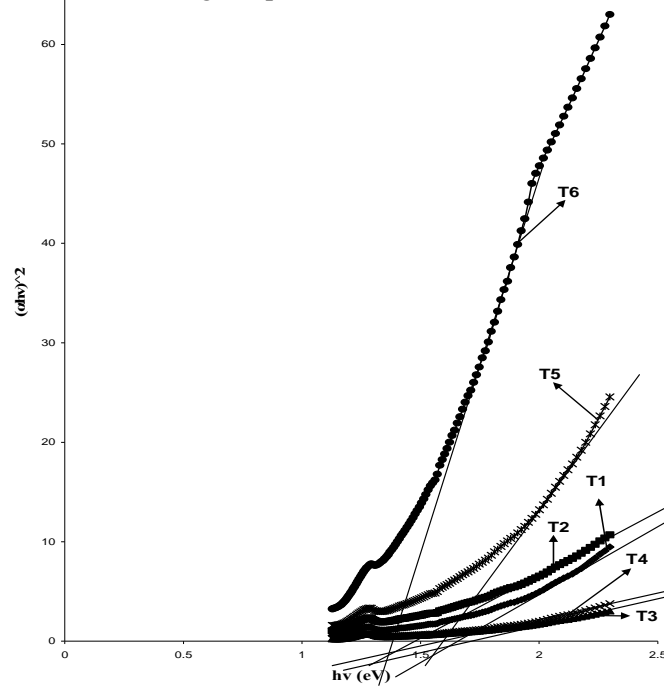


Fig. 5: Plot of Band Gap (Direct) for different Mn concentration and annealing temperatures

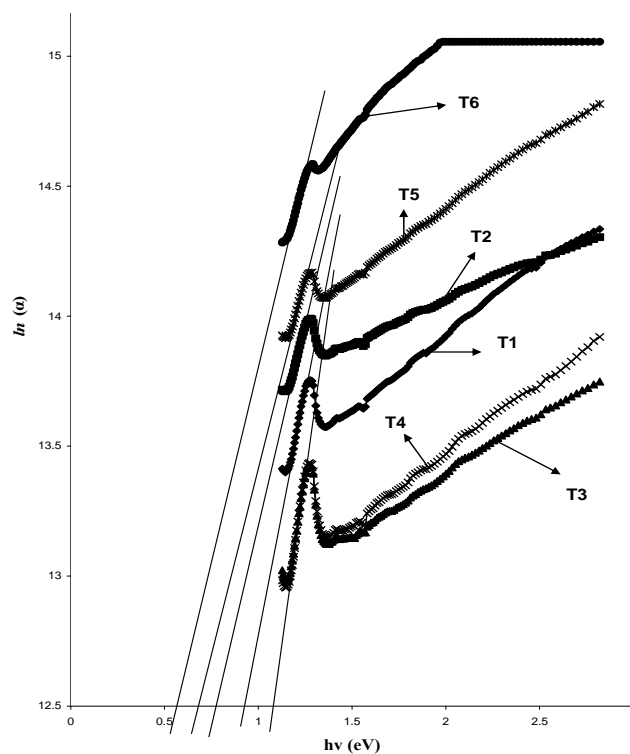


Fig. 6. Determination of Urbach's Energy.

Table 1: Variation of the Band Gap and Urbach's Energy of Mn-ZnO Crystals with Doping Concentration.

Sample	Mass of Manganese Acetate Used (g)	Band Gap (eV)	Urbach's Energy (eV)
T1	5	1.7	0.9
T2	3	1.45	0.75
T3	1	1.75	1.1

Table 2: Variation of the Band Gap and Urbach's Energy of Mn-ZnO Crystals with Annealing Temperature.

Sample	Mass of Manganese Acetate Used (g)	Annealing Temperature (°C)	Band Gap (eV)	Urbach's Energy (eV)
T1	5	As-grown	1.7	0.9
T4	5	200	1.6	1.1
T2	3	As-grown	1.45	0.75
T5	3	200	1.6	0.7
T3	1	As-grown	1.75	1.1
T6	1	200	1.35	0.58

4. Conclusions

The XRD analysis shows that higher concentrations of manganese dopant (i.e. crystals grown with mass of manganese acetate greater than 1g) cause a deviation from the hexagonal wurtzite structure of zinc oxide. This is in agreement with the observations from the FTIR spectra which show Zn-O bonds only for crystals grown with 1g manganese acetate. Higher concentrations of the Mn²⁺ dopant ion gives rise to the formation of synthetic MnO₂ (pyrolusite). The presence of MnO₂ could possibly explain the inconsistent behaviour observed for the absorbance, band gap and Urbach's energy.

References

- [1] R.K. Singhal, M. Dhawan, S. Kumar, S.N. Dolia, Y.T. Xing, E. Saitovitch, *Physica B*. **404**, 3275 (2009).
- [2] I. A. Kowalik, E. Guziewicz, Ł. Wachnicki, K. Kopalko, A. Wójcik, E. Łusakowska, M. Godlewski, *Synchrotron Radiation in Natural Science*. **7**(1-2), 112 (2008).
- [3] G.M. Dalpian, S. Wei, X.G. Gong, A.J.R. da Silva, A. Fazzio, *Solid State Communications*. **138**, 353 (2006).
- [4] Y. Liu, S. Yang, Y. Zhang, D. Bao, *Journal of Magnetism and Magnetic Materials*. **321**, 3406 (2009).
- [5] J.H. Li, D.Z. Shen, J.Y. Zhang, D.X. Zhao, B.S. Li, Y.M. Lu, Y.C. Liu, X.W. Fan, *Journal of Magnetism and Magnetic Materials*. **302**, 118 (2006).

- [6] E. Chikoidze, Y. Dumont, H.J. von Bardeleben, J. Gleize, O. Gorochoy, *Journal of Magnetism and Magnetic Materials*. **316**, e181 (2007)
- [7] J.A. Sans, G. Martínez-Criado, J. Susini, R. Sanz, J. Jensen, I. Minguéz, M. Hernandez-Velez, A. Labrador, P. Carpentier, *Journal of Applied Physics*. **107**, 023507-1 (2010).
- [8] M. Diaconu, H. Schmidt, H. Hochmuth, M. Lorenz, G. Benndorf, D. Spemann, A. Setzer, P. Esquinazia, A. Pöppel, H. von Wenckstern, K.-W. Nielsen, R. Gross, H. Schmid, W. Mader, G. Wagner, M. Grundmann, *Journal of Magnetism and Magnetic Materials* **307**, 212 (2006).
- [9] S. Chattopadhyay, S. Dutta, A. Banerjee, D. Jana, S. Bandyopadhyay, S. Chattopadhyay, A. Sarkar, *Physica B*. **404**, 1509 (2009).
- [10] S. Suwanboon, *Naresuan University Journal*. **16**(2), 173 (2008).
- [11] A. Wójcik, M. Godlewski, E. Guziewicz, R. Minikayev, W. Paszkowicz, *Journal of Crystal Growth*. **310**, 284 (2008).
- [12] R. C. Brundle, C. A. Evans (Jr.), S. Wilson, *Encyclopaedia of Materials Characterization: Surfaces, Interfaces, Thin Films (Materials Characterization Series)*. Butterworth-Heinemann, Stoneham, **MA02180**, 416 (1992).
- [13] J. Coates, *Interpretation of Infrared Spectra, A Practical Approach*; in *Encyclopedia of Analytical Chemistry*, R.A. Meyers (Ed.). John Wiley & Sons Ltd, Chichester. 10815 (2000).
- [14] D. Geetha, T. Thilagavathi, *Digest Journal of Nanomaterials and Biostructures*. **5**(1), 297 (2010).
- [15] K. Nakamoto, *Infrared and Raman Spectra of Inorganic and Coordination Compounds, Parts A and B*. John Wiley & Sons, New York (1997)
- [16] R. Sharma, B.P. Chandra, D.P. Bisen, *Chalcogenide Letters*. **6**(8), 339 (2009).
- [17] B.E. Waren, *X-ray Diffraction*, Addison-Wesley, Reading, MA. (1969)
- [18] O.W. Perez-Lopez, A.C. Farias, N.R. Marcilio, J.M.C. Bueno, *Materials Research Bulletin*. **40**, 2089 (2005).
- [19] R. Yousefi, B. Kamaluddin, *Applied Surface Science*. **256**, 329 (2009).
- [20] A.K. Pradhan, D. Hunter, K. Zhang, J.B. Dadson, S. Mohanty, T.M. Williams, K. Lord, R.R. Rakhimov, U.N. Roy, Y. Cui, A. Burger, J. Zhang, D.J. Sellmyer, *Applied Surface Science*. **252**, 1628 (2005).
- [21] N. Singh, S. Mittal, K.N. Sood, Rashmi, R.K. Gupta, *Chalcogenide Letters*. **7**(4), 297 (2010).
- [22] B.S. Amma, K. Manzoor, K. Ramakrishna, M. Pattabi, *Materials Chemistry and Physics*. **112** 789 (2008).
- [23] S. Tanunchai, S. Towta, N. Mangkorntong, P. Mangkorntong, S. Choopun, *Chiang Mai J. Sci.* **32**(3), 453 (2005).
- [24] R.P. Chahal, S. Mahendia, A.K. Tomar, S. Kumar, *Chalcogenide Letters*. **7**(8), 569 (2010).